COMMUNICATIONS IN NUMERICAL METHODS IN ENGINEERING
Commun. Numer. Meth. Engng (in press)
Published online in Wiley InterScience (www.interscience.wiley.com). DOI: 10.1002/cnm.1001

A simple error estimator for extended finite elements

Stéphane Bordas[1,*,†], Marc Duflot[2] and Phong Le[3]

[1]*Civil Engineering Department, University of Glasgow, Rankine Building, Glasgow G12 8LT, U.K.*
[2]*CENAERO, Avenue Jean Mermoz, 30, B-6041 Gosselies, Belgium*
[3]*Computational Engineering Research Centre, Faculty of Engineering and Surveying, University of Southern Queensland, Australia*

SUMMARY

This short communication presents the idea of an *a posteriori* error estimate for enriched (extended) finite elements (XFEM). The enhanced strain field against which the XFEM strains are compared, is computed through extended moving least-squares smoothing constructed using the diffraction method to preserve the discontinuity. The error estimator is the L_2 norm of the difference of the XFEM strain with the enhanced strain. We prove the concept of the proposed method on a 1D example with a singular solution and a 2D fracture mechanics example and conclude with some future work based on our paradigm. Copyright © 2007 John Wiley & Sons, Ltd.

Received 14 October 2006; Revised 14 February 2007; Accepted 15 February 2007

KEY WORDS: *a posteriori* error estimation; derivative recovery; extended finite element method; intrinsic enrichment; moving least-squares approximation; near-tip enrichment

1. INTRODUCTION

We propose a simple derivative recovery technique and its associated *a posteriori* error estimator, based on the idea of [1] for extended finite-element methods (XFEM). The latter has been used to tackle problems involving discontinuities and singularities [2–5]. Other work on *a posteriori* estimates of enriched finite-element methods is [6].

The idea is to compute an enhanced strain field as an intrinsically extended moving least squares (XMLS) based on the nodal values from the raw XFEM solution. In each element, the local error

*Correspondence to: Stéphane Bordas, Civil Engineering Department, University of Glasgow, Rankine Building, Glasgow G12 8LT, U.K.
†E-mail: stephane.bordas@alumni.northwestern.edu

Contract/grant sponsor: Walloon Region
Contract/grant sponsor: FEDER European funds; contract/grant number: EP1A122030000102

Copyright © 2007 John Wiley & Sons, Ltd.

estimator proposed is the L_2 norm of the difference between the enhanced and the XFEM strain field.

The communication is organized as follows. In Section 2, the extended finite-element method is presented. Section 3 details the recovery and error calculation algorithm. A 1D example of recovery for an equation with a singularity is given in Section 4 and a 2D fracture mechanics problem is presented in Section 5. Section 6 concludes with some further likely developments.

2. EXTENDED FINITE-ELEMENT METHOD

The XFEM [2, 3] is based on partition of unity enrichment [7, 8]. An arbitrary function E (or several) is added to the finite-element approximation to capture essential features of a problem. Similar methods are the generalized finite element method (GFEM) [9, 10] and Nitsche's method [11], equivalent to XFEM [12].

We now recall the form of the XFEM approximation u^h for a scalar function u on an element whose nodes are in set $\mathcal{N}$, while $\mathcal{N}_{\text{enr}}$ is the set of the element's enriched nodes. Let us define the N_I's as the standard finite element shape functions and the $\widetilde{N}_J$ localizing the enrichment functions E. The XFEM approximation at point x in the element writes

$$u(x) = \sum_{I \in \mathcal{N}} N_I(x) u_I + \sum_{J \in \mathcal{N}_{\text{enr}}} \widetilde{N_J}(x) E(x) a_J \tag{1}$$

The u_I are the standard unknowns and the a_J the enrichment coefficients. Introducing this approximation into the weak form governing the problem, one obtains a stiffness matrix which is banded, symmetric, and positive definite.

Let $\mathcal{N}$ be the set of nodes in the XFEM mesh. For linear elastic fracture mechanics problems, define $\mathcal{N}_{\text{cut}}$ as the set of nodes whose support is entirely cut by the crack, they are enriched with function $H(\mathbf{x})$, the modified Heaviside function which takes the value $+1$ above the crack and -1 below the crack. Let $\mathcal{N}_{\text{tip}}$ be the set of nodes contained in a ball of fixed radius, $r_{\text{enr}}^{\text{XFEM}}$, centred on the crack tip. These nodes are enriched by the near-tip branch functions denoted by $[B_\alpha]_{1 \leqslant \alpha \leqslant 4}(\mathbf{x}) = [B_\alpha]_{1 \leqslant \alpha \leqslant 4}(r, \theta)$, which is a basis that spans the near-tip asymptotic fields[‡]

$$\begin{aligned} \mathbf{B}(r, \theta) &\equiv [B_1, B_2, B_3, B_4](r, \theta) \\ &= \left[\sqrt{r} \sin \frac{\theta}{2}, \sqrt{r} \cos \frac{\theta}{2}, \sqrt{r} \sin \frac{\theta}{2} \cos \theta, \sqrt{r} \cos \frac{\theta}{2} \cos \theta \right] \end{aligned} \tag{2}$$

With these definitions, the XFEM approximation for a crack in linear elastic fracture mechanics reads

$$\begin{aligned} \mathbf{u}^h(\mathbf{x}) = &\sum_{I \in \mathcal{N}} N_I(\mathbf{x}) \mathbf{u}_I + \sum_{J \in \mathcal{N}_{\text{cut}}} \widetilde{N}_J(\mathbf{x}) (H(\mathbf{x}) - H(\mathbf{x}_J)) \mathbf{a}_J \\ &+ \sum_{K \in \mathcal{N}_{\text{tip}}} \widetilde{N}_K(\mathbf{x}) \sum_{\alpha=1}^{4} (B_\alpha(\mathbf{x}) - B_\alpha(\mathbf{x}_K)) \mathbf{b}_{\alpha K} \end{aligned} \tag{3}$$

[‡] (r, θ) are the usual polar co-ordinates defined by the crack.

Copyright © 2007 John Wiley & Sons, Ltd.

DOI: 10.1002/cnm

3. RECOVERY BY DIFFRACTED EXTENDED MOVING LEAST SQUARES

Moving least-square (MLS) approximations were originally created by mathematicians to fit and construct surfaces [13] and has been used since the invention of the element-free Galerkin method [14] to construct shape functions for mesh-free methods.

The enhanced derivative is computed as the derivative of the MLS smoothing of the raw XFEM field. The latter shall be indicated with a superscript h, the enhanced by a superscript s (for smooth).

At a node $\mathbf{x}_k$, we note the nodal XFEM displacement vector $\mathbf{u}_k^h = \mathbf{u}^h(\mathbf{x}_k)$. We define the symmetric gradient operator $\mathscr{D}(\cdot)$ transforming the displacements $\mathbf{u}^h$ into the strains $\boldsymbol{\varepsilon}^h$

$$\boldsymbol{\varepsilon}^h = \tfrac{1}{2}(\boldsymbol{\nabla} + \boldsymbol{\nabla}^{\mathrm{T}}) \otimes \mathbf{u}^h = \mathscr{D} \otimes \mathbf{u}^h \tag{4}$$

In the following, quantities in square brackets $[\cdot]$ and curly brackets $\{\cdot\}$ are matrix operators and vectors of nodal values, respectively. Let $\mathbf{x}$ be a point in domain Ω, $n_{\mathbf{x}}$ XMLS points have $\mathbf{x}$ in their domain of influence. Those XMLS points form set $\mathscr{N}_{\mathrm{XMLS}}$. The enhanced displacement and strain fields write

$$\mathbf{u}^s(\mathbf{x}) = \sum_k^{n_{\mathbf{x}}} \Phi_k(\mathbf{x}) u_k^h = [\boldsymbol{\Phi}]^{\mathrm{T}}(\mathbf{x})\{\mathbf{u}^h\} \tag{5}$$

$$\boldsymbol{\varepsilon}^{\mathrm{s}}(\mathbf{x}) = \sum_k^{n_{\mathbf{x}}} \mathscr{D}(\Phi_k)(\mathbf{x}) u_k^h = [\mathscr{D}](\mathbf{x})\{\mathbf{u}^h\} \tag{6}$$

$\Phi_k(\mathbf{x})$ is the value of the MLS shape function associated with node k at point $\mathbf{x}$. $\left\{\mathbf{u}^h\right\}$ and $[\boldsymbol{\Phi}]$ are $n_{\mathbf{x}} \times 1$ vectors, $[\mathscr{D}]$ is a $3 \times n_{\mathbf{x}}$ matrix in 2D and a $6 \times n_{\mathbf{x}}$ matrix in 3D. The $n_{\mathbf{x}}$ MLS shape functions that are non-zero at point $\mathbf{x}$ write

$$(\Phi_k(\mathbf{x}))_{1 \leqslant k \leqslant n_{\mathbf{x}}} = \mathbf{c}(\mathbf{x})^{\mathrm{T}} \mathbf{p}(\mathbf{x}_k) w_k(\mathbf{x}) \tag{7}$$

with

$$\mathbf{c}(\mathbf{x}) = \mathbf{A}(\mathbf{x})^{-1} \mathbf{p}(\mathbf{x}) \tag{8}$$

- $\mathbf{p}$ is the vector of m basis functions defined in Table I. For the fracture mechanics problem, we use the enriched linear basis given in the last row of the table. For the 1D example, we use the one but last row.
- $\mathbf{A}$ is an $m \times m$ matrix which has to be inverted everywhere the MLS functions are computed: $\mathbf{A}(\mathbf{x}) = \sum_{k=1}^{n_{\mathbf{x}}} w_k(\mathbf{x}) \mathbf{p}(\mathbf{x}_k) \mathbf{p}^{\mathrm{T}}(\mathbf{x}_k)$.
- w_k is the weight function associated with point $\mathbf{x}_k$. It is modified to introduce a discontinuity in the approximation, if needed, by the diffraction criterion.

Remark
Because of the presence of the near-tip fields in the $\mathbf{p}$ vector defined above, we coin the recovery method XMLS.

Remark
Due to intrinsic enrichment of the MLS basis, the near-tip fields can be reproduced by the MLS approximation.

Copyright © 2007 John Wiley & Sons, Ltd.

DOI: 10.1002/cnm

Table I. Some possible basis functions used for MLS approximations.

	1D	2D	3D
Constant	$[1]$	$[1]$	$[1]$
Linear	$[1, x]$	$[1, x, y]$	$[1, x, y, z]$
Quadratic	$[1, x, x^2]$	$[1, x, y, x^2, y^2, xy]$	$[1, x, y, z, x^2, y^2, z^2, xy, xz, yz]$
Linear + enrichment	$[1, x, \text{sign}(x)\sqrt{\lvert x\rvert}]$	—	—
Linear + tip	—	$[1, x, y, [B_\alpha(r, \theta)]_{1\leqslant\alpha\leqslant4}]$	$[1, x, y, z, [B_\alpha(r, \theta)]_{1\leqslant\alpha\leqslant4}]$

Note: The branch functions are $\mathbf{B} \equiv [B_\alpha(r, \theta)]_{1\leqslant\alpha\leqslant4} \equiv [B_1, B_2, B_3, B_4](r, \theta) = [\sqrt{r}\sin\frac{\theta}{2}, \sqrt{r}\cos\frac{\theta}{2}, \sqrt{r}\sin\frac{\theta}{2}\cos\theta, \sqrt{r}\cos\frac{\theta}{2}\cos\theta]$. (r, θ) are the polar co-ordinates defined by the crack tip and the tangent direction to the crack. r is the distance to a point in space to the tip and θ the angle between the crack direction and the vector 'tip to point'.

In this work, the fourth-order spline weight function is chosen. In 1D, if s is the normalized distance between node x_k and point x in the computational domain

$$s = \left|\frac{x - x_k}{d_k}\right| \tag{9}$$

where d_k is the size of the support domain of node x_k. The quartic spline writes

$$f_4(s) = \begin{cases} 1 - 6s^2 + 8s^3 - 3s^4 & \text{if } |s|\leqslant 1 \\ 0 & \text{if } |s| > 1 \end{cases} \tag{10}$$

In the 2D example, we use circular domains of influence, such that

$$w_k(\mathbf{x}) = f_4\left(\frac{\|\mathbf{x} - \mathbf{x}_k\|}{d_k}\right) \tag{11}$$

To account for the presence of a discontinuity in the approximation, s is computed differently than above. The diffraction method was introduced in [15, 16] to represent discontinuities in the element-free Galerkin method (see Figure 1). When a discontinuity is to be described, if it hides a point, the weight of a node at this point is diminished. When the line segment [IX] of Figure 1 is bissected by a crack, s of Equation (11) is replaced by the normalized length of the shortest path from I to X passing by a point of the front (path ICX in Figure 1).

$$s = \frac{\|\mathbf{x} - \mathbf{x}_c\| + \|\mathbf{x}_c - \mathbf{x}_i\|}{R_i} \tag{12}$$

The weight function of nodes I and J are then continuous except across the discontinuity; moreover, the domain of influence of node I wrap around the tip. The shape functions' derivatives are obtained by differentiating (7), which involves extra matrix computations, see Reference [14] for details.

3.1. Error estimate

On element Ω_q, the *approximate error* between the raw and the smoothed solution is measured by the L_2 norm of the difference between the raw XFEM derivative and the enhanced derivative.

Copyright © 2007 John Wiley & Sons, Ltd.

DOI: 10.1002/cnm

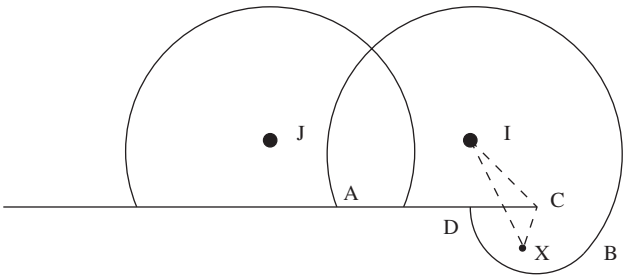


Figure 1. Diffraction method for introducing discontinuities in moving least-squares approximations.

The global approximate error is measured by the sum of the element-wise errors on the n_{elt} elements of the mesh

$$e^{hs}_{\Omega_q} = \sqrt{\int_{\Omega_q} \|\boldsymbol{\varepsilon}^h(\mathbf{x}) - \boldsymbol{\varepsilon}^s(\mathbf{x})\|^2 \, \mathrm{d}\mathbf{x}} \tag{13}$$

$$e^{hs} = \sqrt{\sum_{q=1}^{n_{\text{elt}}} e^{hs\,2}_{\Omega_q}} \tag{14}$$

Define $e^{he}_{\Omega_q}$ as the L_2 norm of the difference between the raw XFEM solution and the exact solution on element Ω_q. This is the *exact error*

$$e^{he}_{\Omega_q} = \sqrt{\int_{\Omega_q} \|\boldsymbol{\varepsilon}^h(\mathbf{x}) - \boldsymbol{\varepsilon}^{\text{exact}}(\mathbf{x})\|^2 \, \mathrm{d}\mathbf{x}} \tag{15}$$

Similarly, the global exact error can be written as

$$e^{he} = \sqrt{\sum_{q=1}^{n_{\text{elt}}} e^{he\,2}_{\Omega_q}} \tag{16}$$

3.2. *Effectivity*

The global error effectivity index of the estimator is defined as the *ratio of the approximate error to the exact error*

$$\theta = \frac{e^{hs}}{e^{he}} \tag{17}$$

The effectivity index measures how close the approximate error is to the exact error. An effectivity of one would be reached if the approximate error were exactly equal to the exact error. This is, in practice, not achievable, but, the closer the effectivity is to unity, the better the indicator. In order for an error indicator to be valid, the approximate error it indicates should converge to the exact error as the mesh size goes to zero. We will see in the numerical examples that this is the case for the proposed indicator.

Copyright © 2007 John Wiley & Sons, Ltd.

DOI: 10.1002/cnm

4. ONE-DIMENSIONAL NUMERICAL EXAMPLE

To explain the methodology and show the need for enrichment of the MLS basis, we first examine a simple 1D example where the analytical solution has a singular derivative and is given by

$$\forall x \in \mathbb{R}, \quad u(x) = \text{sign}(x)\sqrt{(|x|)}(1 + x^2/100) \tag{18}$$

Note first that the derivative of u is singular at $x = 0$. We define a piece-wise linear solution to this problem by linear interpolation between exact nodal values, for 11 equispaced nodes along domain $[-4.5; 4.5]$. This solution will be known as the *raw* solution. We then compute an enhanced derivative using both a linear $[1, x]$ basis and an enriched MLS basis $[1, x, \text{sign}(x)\sqrt{(|x|)}]$. Figure 2 shows the shape functions and their derivatives for both bases and Figure 3 the results of the enhancement (smoothing). The nodal (raw) values of Figure 2(a) are multiplied by the derivatives of the shape functions shown in Figure 2(c) and (d) to obtain the enhanced derivatives of Figure 3(b). Note that the raw solution is piece-wise linear and has discontinuous derivatives across elements, as opposed to the enhanced derivatives, which are smooth. When the singularity is added to the MLS basis, the enhanced derivative respects the singularity. On the other hand, when the linear MLS basis is used alone, the MLS smoothing is insufficient to correctly capture the singularity in the solution's derivative.

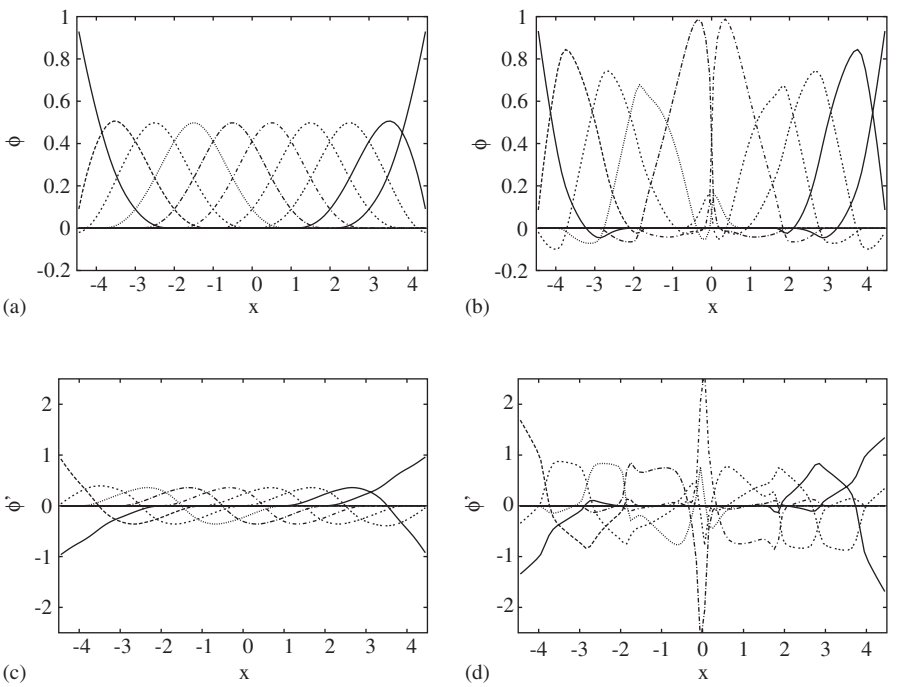


Figure 2. One-dimensional linear and enriched MLS shape functions and their derivatives: (a) linear basis; (b) enriched basis; (c) derivative for linear basis; and (d) derivative for enriched basis.

Copyright © 2007 John Wiley & Sons, Ltd.

DOI: 10.1002/cnm

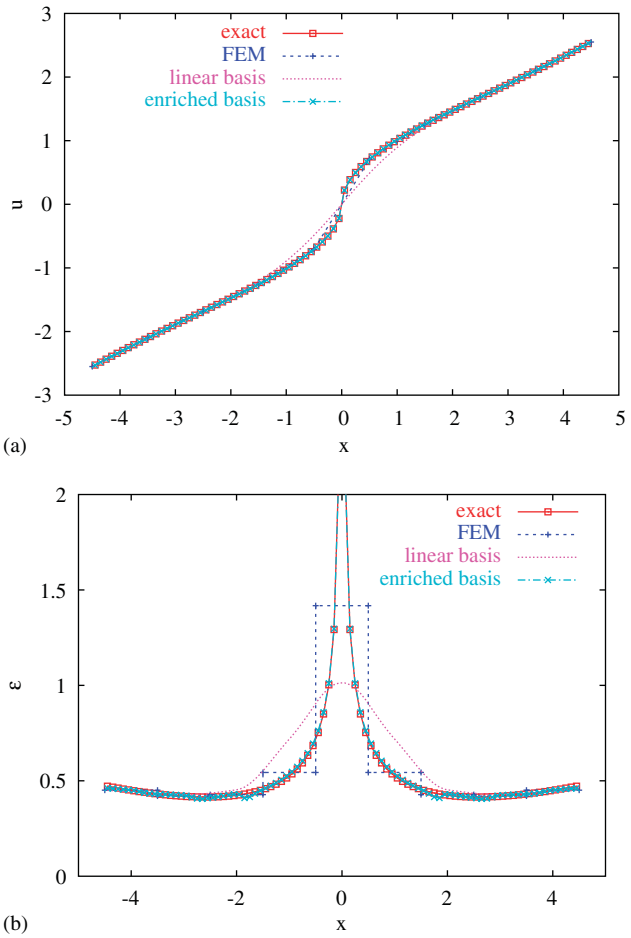


Figure 3. Why do we need extra terms in the MLS approximation? Comparison of the raw FEM and raw FEM derivatives to the enhanced derivatives obtained with a linear MLS basis and extended MLS (XMLS) basis: (a) comparison of the raw, linear-basis and enriched-basis-enhanced solution to the exact solution and (b) comparison of the derivatives of the FEM, linear-basis and enriched-basis-enhanced derivatives.

5. MODE I NEAR-TIP CRACK PROBLEM

This section tests the error estimate on a simple fracture mechanics problem. The domain is a biunit square (bottom left point co-ordinates $[-1, 1]$; top right point co-ordinates $[1, 1]$). XFEM nodes in a disk of radius 0.1, centred on the crack tip are enriched with the near-tip fields $[B_\alpha]_{1\leqslant\alpha\leqslant4}$ given in Equation (2). A horizontal edge crack of unit length is located along the line $y = 0$, the crack tip is at $(0, 0)$. On the boundary of the domain, a traction field equivalent to uniaxial tension applied at infinity is applied.

Copyright © 2007 John Wiley & Sons, Ltd.

DOI: 10.1002/cnm

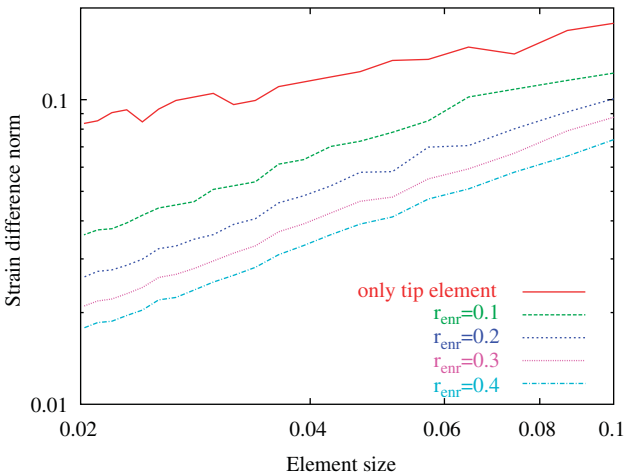


Figure 4. Mode I structured mesh: strain difference convergence with mesh refinement. See Table II for the values of the convergence rates. The larger the enrichment radius, the lower the error and the more monotonic the convergence. If only the tip element is enriched (geometrical enrichment), the convergence rate is 0.46022, for an enrichment radius of 0.4 it reaches 0.91052, close to the optimum.

The mesh is a structured mesh of linear triangular elements shown in Plate 1(a). The raw XFEM strain field is shown in Plate 1(b), where the discontinuities across element faces is clear. Plate 1(c) shows the raw XFEM displacements at all the XFEM nodes. These nodes form the set $\mathcal{N}_{\text{XMLS}}$ that are used to compute the enhanced strain field of Plate 1(d). Note that this enhanced strain field is very smooth compared to the raw XFEM strains. This smoothness is even more obvious from Plate 1(e), which shows the y component of the raw and enhanced strain fields along line $x = 0$. Both strain fields respect the singularity: the raw XFEM strain field because of the near-tip enrichment and the enhanced strain field because of the enriched MLS approximation. Plate 1(f) finally shows the distribution of the L_2 norm of the difference between the raw XFEM strain field and the enhanced strain field in the domain. This norm represents the error made by the XFEM approximation when compared to the enhanced solution.

It is clear from Plate 1(b) and (e) that the raw strain field from XFEM is piece-wise continuous while the recovered strain field, computed from the XFEM nodal displacements of Plate 1(c) are smooth, and very close to the exact solution, even on this moderately fine mesh.

The norm is plotted on each element. We observe that the error is concentrated around the crack tip, as expected. Figure 4 shows the convergence of the approximate error to zero: the convergence rate is close to the optimal rate of 1. It is, however, fundamental to check that not only this L_2 norm of the approximate error converges to zero as the mesh size goes to zero, but also that the *the approximate error converges to the exact error as the mesh size tends to zero*. This is verified by plotting the effectivity index as a function of the characteristic mesh size, in Figure 5. We see that the *effectivity index converges to unity as the mesh size goes to zero*, therefore, the approximate error converges to the exact error, and the proposed indicator is valid.

Copyright © 2007 John Wiley & Sons, Ltd.

DOI: 10.1002/cnm

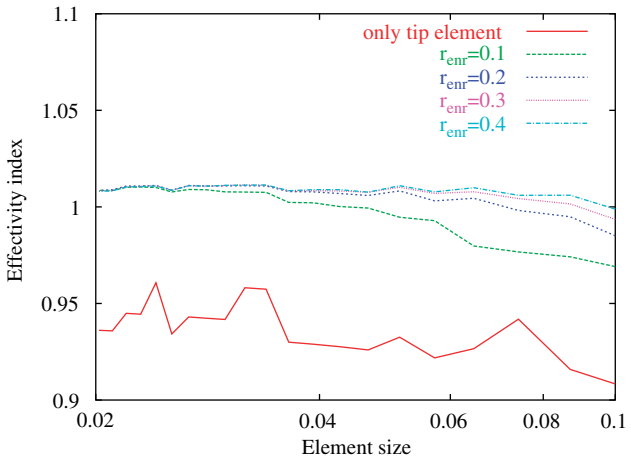


Figure 5. Mode I problem, structured mesh: effectivity index for various XFEM enrichment radii. Enriching only the tip element causes an ineffective error indicator non-convergent to 1. For coarse meshes, higher values of the enrichment radius increase the effectiveness of the indicator. Upon mesh refinement, whatever the enrichment radius, the effectiveness curves meet in the close vicinity of unity.

Table II. Mode I problem, convergence for various XFEM enrichment radii.

Enrichment radius: $r_{\text{enr}}^{\text{XFEM}}$	Convergence rate
Only tip element	0.46022
0.1	0.81271
0.2	0.86728
0.3	0.90644
0.4	0.91052

See also Figure 4. Close to optimal convergence is attained for a fixed area enrichment. The results tend to show that the rate of 1 would be reached if the whole component were enriched.

In Figures 4 and 5, five convergence curves are shown, for four values of the XFEM enrichment radius[§] and one for topological enrichment (only the tip element is enriched). Note that the higher the enrichment radius, the lower the error, the straighter the convergence line, and the closer to optimal the convergence rate is, as summarized in Table II.

Remark

Note from Figures 4 and 5 that the optimal convergence rate and effectivity are maintained only if a *fixed area around the crack tip is enriched* during mesh refinement. If only the crack tip element

[§] We note $r_{\text{enr}}^{\text{XFEM}}$ the enrichment radius. Nodes located within a ball of radius $r_{\text{enr}}^{\text{XFEM}}$, centred on the crack tip are enriched with the near-tip fields.

Copyright © 2007 John Wiley & Sons, Ltd.

DOI: 10.1002/cnm

is enriched, the convergence rate is 0.46022, close to $1/2$[¶] and the effectivity index shows an oscillatory pattern reaching 93% for the finest mesh.

Remark
It is interesting to note that the effectivity *e versus* mesh size *h* curves become closer to the horizontal line $e=1$ with increasing enrichment radius. For coarse meshes, large enrichment radii are necessary to obtain an effective indicator. This is expected, as for coarse meshes, the tip enrichment takes over the standard FEM approximation, which in itself is poorly suited to represent the near-tip behaviour. As the mesh is refined, the standard FEM part of the approximation becomes more important compared to the enriched part, which explains the effectivity curves all meeting in the vicinity of 1 for small *h*'s.

6. CONCLUSIONS AND EXTENSIONS

We showed in this communication that an XMLS technique with diffraction could provide an enhanced solution subsequently employed to define a local error estimator and a remeshing criterion. A proof of concept on a simple 1D example with a singularity and a 2D crack problem shows that the technique is sound and that the effectivity of the error indicator converges to unity as the mesh size goes to zero as long as a fixed area is enriched around the crack tip, as the mesh is refined. The next steps are to apply it to more complex 2D and 3D discontinuous and singular problems. Additionally, comparing the estimator with existing estimators by Zienkiewicz and Zhu [17] will shed more light on the possible usages of the proposed method.

ACKNOWLEDGEMENTS

The first author wishes to thank Dr Raphaël Bonnaz for very helpful discussions on error estimates during their common time at the Laboratory of Structural and Continuum Mechanics at EPFL, Lausanne, Switzerland. He also wishes to thank the whole LSC team for welcoming him between years 2003 and 2006. The guidance of Professor Thomas Zimmermann during those years is especially acknowledged. The support of the Walloon Region and FEDER European funds under contract No. EP1A122030000102 for M. Duflot is gratefully acknowledged.

REFERENCES

1. Tabbara M, Blacker T, Belytschko T. Finite element derivative recovery by moving least square interpolants. *Computer Methods in Applied Mechanics and Engineering* 1994; **117**:211–223.
2. Belytschko T, Black T. Elastic crack growth in finite elements with minimal remeshing. *International Journal for Numerical Methods in Engineering* 1999; **45**:601–620.
3. Moës N, Dolbow J, Belytschko T. A finite element method for crack growth without remeshing. *International Journal for Numerical Methods in Engineering* 1999; **46**:131–150.
4. Bordas S, Moran B. Enriched finite elements and level sets for damage tolerance assessment of complex structures. *Engineering Fracture Mechanics* 2006; **73**:1176–1201.
5. Bordas S, Nguyen VP, Dunant C, Nguyen-Dang H, Guidoum A. An extended finite element library. *International Journal for Numerical Methods in Engineering* 2007, in press.

[¶]The strength of the crack tip stress singularity. This corroborates the findings of References [18, 19].

Copyright © 2007 John Wiley & Sons, Ltd.

DOI: 10.1002/cnm

6. Strouboulis T, Zhang L, Wang D, Babuška I. A posteriori error estimation for generalized finite element methods. *Computer Methods in Applied Mechanics and Engineering* 2006; **195**(9–12):852–879.
7. Melenk JM, Babuška I. The partition of unity finite element method: basic theory and applications. *Computer Methods in Applied Mechanics and Engineering* 1996; **139**:289–314.
8. Babuška I, Melenk I. Partition of unity method. *International Journal for Numerical Methods in Engineering* 1997; **40**(4):727–758.
9. Strouboulis T, Babuška I, Copps K. The design and analysis of the generalized finite element method. *Computer Methods in Applied Mechanics and Engineering* 2000; **181**:43–69.
10. Strouboulis T, Copps K, Babuška I. The generalized finite element method: an example of its implementation and illustration of its performance. *International Journal for Numerical Methods in Engineering* 2000; **47**(8): 1401–1417.
11. Hansbo A, Hansbo P. A finite element method for the simulation of strong and weak discontinuities in solid mechanics. *Computer Methods in Applied Mechanics and Engineering* 2004; **193**(33–35):3523–3540.
12. Areias PMA, Belytschko T. A comment on the article 'A finite element method for simulation of strong and weak discontinuities in solid mechanics'. *Computer Methods in Applied Mechanics and Engineering* 2006; **195**(9–12):1275–1276.
13. Lancaster P, Salkauskas K. Surfaces generated by moving least squares methods. *Mathematics of Computation* 1981; **37**:141–158.
14. Belytschko T, Lu YY, Gu L. Element-free Galerkin methods. *International Journal for Numerical Methods in Engineering* 1994; **37**:229–256.
15. Belytschko T, Krongauz Y, Fleming M, Organ D, Liu WK. Smoothing, accelerated computations in the element-free Galerkin method. *Journal of Computational and Applied Mathematics* 1996; **74**:111–126.
16. Organ D, Fleming M, Terry T, Belytschko T. Continuous meshless approximations for nonconvex bodies by diffraction and transparency. *Computational Mechanics* 1996; **18**:225–235.
17. Zienkiewicz OC, Zhu JZ. A simple error estimator and adaptive procedure for practical engineering analysis. *International Journal for Numerical Methods in Engineering* 1987; **24**:337–357.
18. Laborde P, Pommier J, Renard Y, Salaun M. High order extended finite element method for cracked domains. *International Journal for Numerical Methods in Engineering* 2005; **64**:354–381.
19. Béchet E, Minnebo H, Moës N, Burgardt B. Improved implementation and robustness study of the X-FEM for stress analysis around cracks. *International Journal for Numerical Methods in Engineering* 2006; **67**:1641–1669.

Copyright © 2007 John Wiley & Sons, Ltd.

DOI: 10.1002/cnm

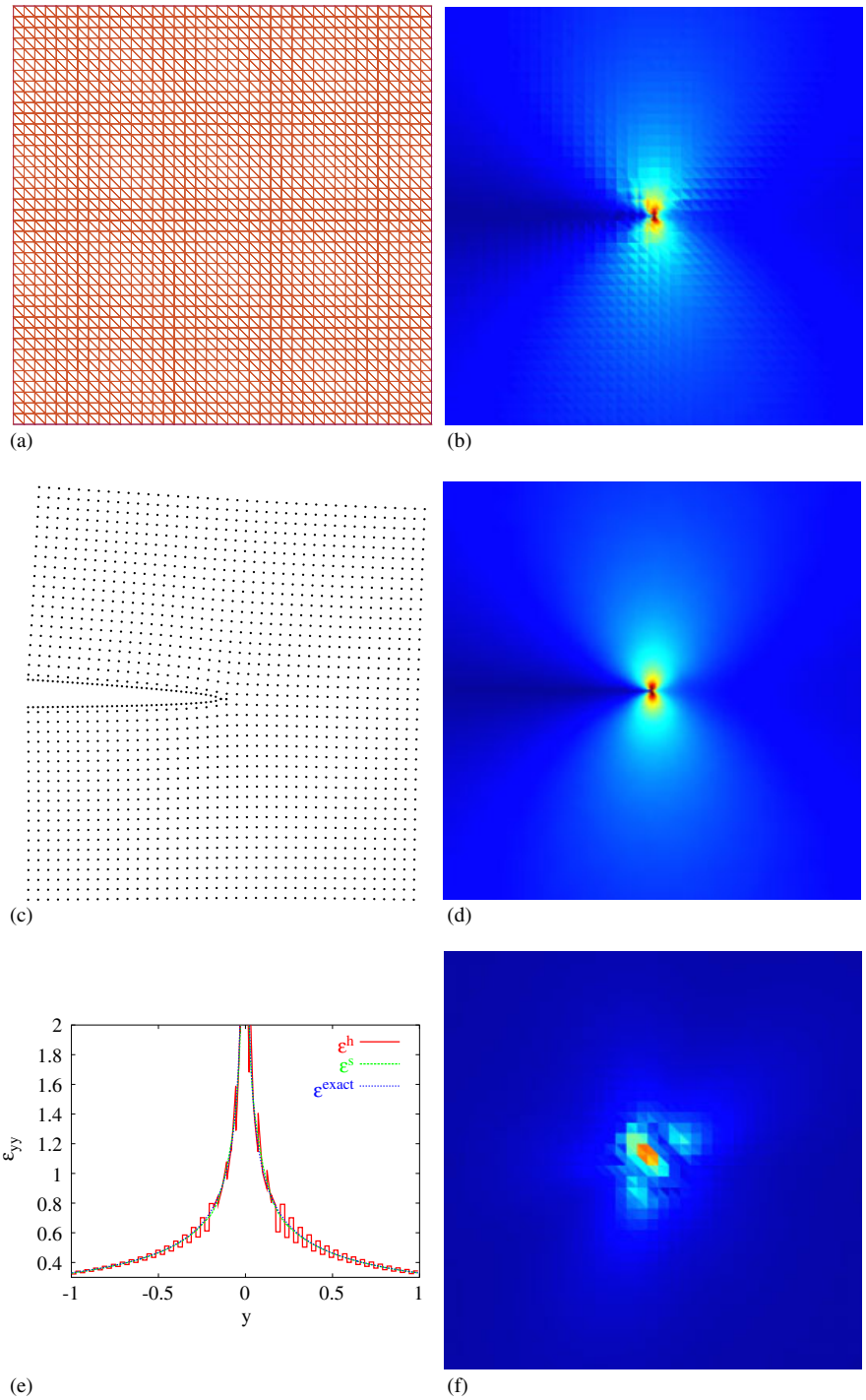


Plate 1. Results for a structured, moderately fine mesh: (a) XFEM mesh; (b) raw strain field; (c) displacement of the nodes in $\mathcal{N}_{\text{XMLS}}$. Only the nodes are represented; (d) XMLS-recovered strain field; (e) $\varepsilon_{yy}(x=0)$; and (f) distribution of $e^{hs}_{\Omega_q}$ of Equation (13) on the mesh.

Copyright © 2007 John Wiley & Sons, Ltd.

DOI: 10.002/cnm